Dalton Transactions

Accepted Manuscript

ROYAL SOCIETY OF CHEMISTRY

www.rsc.org/dalton

Journal Name

COMMUNICATION

Structure, luminescence properties and energy transfer of Tb^{3+}-Eu^{3+} codoped $LiBaB_9O_{15}$ phosphors

Received 00th January 20xx,
Accepted 00th January 20xx

DOI: 10.1039/x0xx00000x

www.rsc.org/

Ting Li, Panlai Li*, Zhijun Wang*, Shuchao Xu, Qiongyu Bai, Zhiping Yang

Abstract: A series of single-composition phosphors $LiBaB_9O_{15}:Tb^{3+}$, Eu^{3+} have been prepared via a high-temperature solid-state reaction process. The structure and luminescence properties of phosphors are described. $LiBaB_9O_{15}:Tb^{3+}$ phosphor shows the characteristic green emission, and the peak locates at 551 nm, which corresponds to the $^5D_4 \rightarrow {}^7F_5$ transition of Tb^{3+}. $LiBaB_9O_{15}:Eu^{3+}$ phosphor presents an obvious red emission, and the peak locates at 617 nm, which is ascribed to the $^5D_0 \rightarrow {}^7F_2$ transition of Eu^{3+}. The highly intense red emission peaks of the Eu^{3+} ions were attributed to an effective energy transfer from the Tb^{3+} to Eu^{3+} ions in $LiBaB_9O_{15}:Tb^{3+}$, Eu^{3+}, which have been justified through the luminescence spectra and the fluorescence decay dynamics. The results mean that $LiBaB_9O_{15}:Tb^{3+}$, Eu^{3+} phosphor might have potential applications as a red emitting phosphor for white LEDs.

1. Introduction

Tremendous attentions have been attracted to white light-emitting diodes (white LEDs) for the advantages such as high energy efficiency, long operation lifetime, small size and environmental friendliness.[1-5] The majority of white-LEDs use a combination of a blue InGaN chip and yellow-emitting $Y_3Al_5O_{12}:Ce^{3+}$ (YAG:Ce^{3+}) phosphor.[6,7] They are also characterized by cool white color temperatures, e.g., correlated color temperature (CCT) 7756 K, and poor color rendering indices (CRI, Ra), e.g., Ra =75.2 and the lack of red-light contribution also obstructs its extension for more vivid application.[8-10] In recent years, the near ultraviolet LEDs (n-UV LEDs, 370-410 nm) have elicited interest since they can potentially provide improved color temperatures and Ra's in comparison with white-LEDs.[11-14] This is because of their high color-rendering properties and tuneable color temperatures by changing the R/G/B or Y/B ratios. The n-UV excitable trichromatic phosphors have been elucidated and investigated for many hosts. According to Chiu et al., a near-UV LED chip combining trichromatic $CaAlSiN_3:Eu^{2+}$ (red), $(Ba,Sr)_2SiO_4:Eu^{2+}$ (green), and $Ca_2PO_4Cl:Eu^{2+}$ (blue) emitting phosphors provides a relatively high CRI of Ra=93.4 and low CCT of 4590 K. Kim et al. reported that $Ba_3MgSi_2O_8:Eu^{2+}$, Mn^{2+} can be used as a phosphor for fabrication of a warm white-LED.[15-21] The generation of white light emission largely depends on the energy transfer of excitation energy between rare-earth ions. Accordingly, the energy transfer from a large number of ion pairs has been investigated because of relatively bright room-temperature fluorescence in the visible optical region.[22–33]

Up to now, many researchers have reported the energy transfer from Tb^{3+} to Eu^{3+}. For example, Mengmeng Jiao et al. reported that the energy transfer from the Tb^{3+} to Eu^{3+} in $Ca_3Bi(PO_4)_3$ phosphors.[34] Zhenhe Xu et al. reported that the energy transfer from the Tb^{3+} to Eu^{3+} in $NaY(MoO_4)_2$ phosphors.[35] Xiaoming Liu et al. reported that the energy transfer from Tb^{3+} to Eu^{3+} ions in $YNbO_4$ phosphors,[36] and it can emit red emission through efficiently energy transfer from Tb^{3+} to Eu^{3+}. Huan Jiao et al. reported that the luminescent properties of Eu^{3+} and Tb^{3+} in $Zn_3Ta_2O_8$ phosphors.[37] As we all know, lithium barium borate $LiBaB_9O_{15}$ has a low cost, high physical and chemical stability , moreover, it can be doped with a high concentration of Eu^{3+} without concentration quenching.[38] Therefore, $LiBaB_9O_{15}$ is selected as host material for red emitting phosphor in n-UV white LEDs. To the best of our knowledge, the luminescence properties of $LiBaB_9O_{15}:Tb^{3+}$, Eu^{3+} has not been reported in the literature. In this study, we have demonstrated the luminescence properties and energy transform of red emitting $LiBaB_9O_{15}:Tb^{3+}$, Eu^{3+} phosphors. X-ray diffraction, luminescence, CIE coordinates and decay curves were utilized to characterize the phosphors. $LiBaB_9O_{15}:Tb^{3+}$, Eu^{3+} might have potential application as a red emitting phosphor for UV-excited white-LEDs via energy transfer from Tb^{3+} to Eu^{3+}.

2. Experimental

2.1. Materials and synthesis

[a] College of Physics Science & Technology, Hebei Key Lab of Optic-Electronic Information and Materials, Hebei University, Baoding 071002, China
+li_panlai@126.com; wangzj1998@126.com

Electronic Supplementary Information (ESI) available: [details of any supplementary information available should be included here]. See DOI: 10.1039/x0xx00000x

A series of $LiBaB_9O_{15}$:Tb^{3+}, Eu^{3+} powder samples were prepared by a high temperature solid-state reaction process. The starting materials H_3BO_3 (analytical reagents, A.R.), $BaCO_3$ (A.R.), Li_2CO_3 (A.R.), Tb_4O_7 (99.99%) and Eu_2O_3 (99.99%) were weighed by an electronics scales with a 0.0001g accuracy. The doping contents of Eu^{3+} and Tb^{3+} were selected as 0.001-0.01mol in $LiBaB_9O_{15}$, respectively. Typically, stoichiometric amounts of H_3BO_3, $BaCO_3$, Li_2CO_3, Tb_4O_7 and Eu_2O_3 were thoroughly mixed in an agate mortar for 30 min. The as-obtained mixing solid powders was transferred into an alumina crucible, and the sintered at 850 °C for 2 h in air. After firing, the samples were cooled to room temperature in the furnace and ground again into powder for subsequent use.

2.2. Materials characterization

The crystal structure of the as-synthesized samples was determined by using X-Ray Powder Diffraction (XRD) (D/max-rA, Cu Kα, 40 kV, and 30 mA); the Findit software and Crystalmaker software were used for the phase information. The photoluminescence (PL) and PL excitation (PLE) spectra of the samples were analyzed by using a F4600 Spectrofluorometer equipped with a 450-W Xe light source. The Commission International de l'Eclairage (CIE) chromaticity coordinates for all samples were measured by a PMS-80 UV-VIS-NEAR IR spectra analysis system. The decay curves were recorded using a 450-W Xe lamp was used as the excitation source (HORIBA, FL-1057). Photoluminescence absolute quantum efficiency (QE) was measured by an absolute PL quantum yield measurement system (HORIBA, FL-1057). All the luminescent characteristics of the phosphors were investigated at room temperature.

3. Results and discussion

3.1. Crystal structure of $LiBaB_9O_{15}$:Tb^{3+}, Eu^{3+}

The XRD patterns of as-prepared $LiBaB_9O_{15}$:*x*Tb^{3+}, 0.02Eu^{3+} and $LiBaB_9O_{15}$:0.02Tb^{3+}, *y*Eu^{3+} samples are measured, and the similar results are observed. As a representative, Figure 1 shows the XRD patterns of $LiBaB_9O_{15}$:*x*Tb^{3+}, 0.02Eu^{3+} and the standard data for $LiBaB_9O_{15}$ (JCPDS#47-0341). All of the diffraction peaks of the XRD patterns can be indexed as pure phase, and coincide well with the standard data of $LiBaB_9O_{15}$. The absence of any detectable peak shift or other phase in the XRD patterns indicates that the pure $LiBaB_9O_{15}$ phase can be obtained under the above conditions by this simple method. The strong and sharp diffraction peaks of the samples indicate that the as-obtained $LiBaB_9O_{15}$ samples are well crystallized. The results show that different dopant concentrations do not result in any other phase except the main phase.

$LiBaB_9O_{15}$ crystallizes in a trigonal/rhombohedral system with space group *R-3c:H* and with four chemical formula units per unit cell. The dimensions of the unit cell are a=11.02230 Å, b=11.02230 Å, c =17.10600 Å and V=1782.59 $Å^3$. Figure 2 shows the crystal structure of $LiBaB_9O_{15}$, the basic structural features of the $LiBaB_9O_{15}$ crystal include Li^+ ions, $(BO_3)^{3-}$ groups, and Ba-O groups. The cations together with the Tb^{3+} and Eu^{3+} ions are distributed in a statistical manner on the 6a sites, while the B atoms are fixed on 18b sites. The doped rare earth ions substituting for the Ba^{2+} ions occupy a distorted dodecahedron of oxygen ions. The ionic radii for Li^+ (coordination number (CN) = 2), Ba^{2+} (CN=4), and B^{3+} (CN=4) are 0.59 Å, 1.34 Å and 0.2 Å, respectively.[35] The ionic radii of dopant Tb^{3+} (CN=4) and Eu^{3+} (CN=4) are 0.923 Å and 0.950 Å, respectively. The ionic radii of Tb^{3+}, Eu^{3+} are both close to the ionic radii of Ba^{2+}. It is believed that Tb^{3+} and Eu^{3+} ions are substituted in the sites of Ba^{2+} in the $LiBaB_9O_{15}$ host.

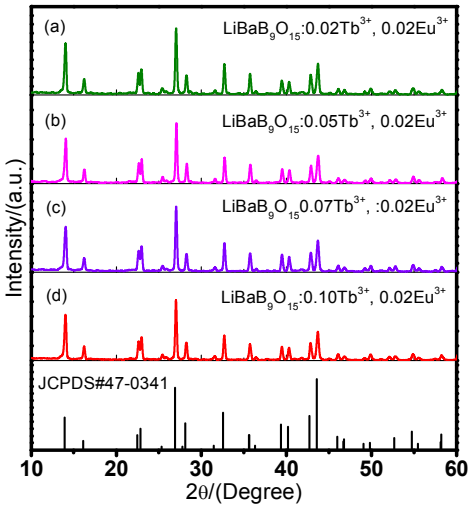

Figure 1 XRD patterns of as-prepared $LiBaB_9O_{15}$: xTb^{3+}, 0.02Eu^{3+} samples and the standard data for $LiBaB_9O_{15}$ (JCPDS#47-0341)

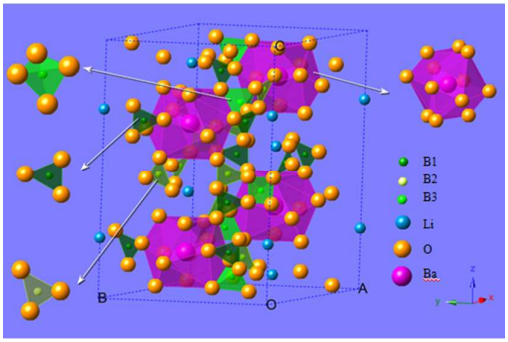

Figure 2 Crystal structure of $LiBaB_9O_{15}$ in a trigonal/rhombohedral system with space group *R-3c:H*.

3.2. Luminescence properties and energy transfer of $LiBaB_9O_{15}$:Tb^{3+}, Eu^{3+}

Figure 3 shows the PL and PLE spectra of $LiBaB_9O_{15}$:0.02Eu^{3+} (a) and $LiBaB_9O_{15}$:0.02Tb^{3+} (b), inset (a) and inset (b) show the intensity changes with concentration in $LiBaB_9O_{15}$:*x*Tb^{3+} and $LiBaB_9O_{15}$:*y*Eu^{3+}, respectively. It can be seen from the inset (b), $LiBaB_9O_{15}$:*x*Tb^{3+} shows the maximum intensity, so the optimal concentration of Tb^{3+} is 0.02. In order to facilitate research, we also determined Eu^{3+} as 0.02 although $LiBaB_9O_{15}$:*x*Eu^{3+} has no optimum concentration, which can be seen from the inset (a). For $LiBaB_9O_{15}$:0.02Eu^{3+}, the excitation spectrum of the samples consists of a broad band from

240 to 260 nm with a maximum at 255 nm and numbers of line excitation peaks among which 395 nm is a very sharp one assigned to the f-f transitions of Eu^{3+} $4f^6$ configuration. [39,40] The broad excitation bands peaking at 255 nm is corresponds to charge transfer state. Under optimal excitation wavelength at 395 nm, the sample exhibits a red emission band with maximum emission at 617 nm, which originates from the intra-4f transitions of Eu^{3+} ion. The sharp lines at 594 nm and 617 nm are assigned to the $^5D_0 \rightarrow {}^7F_1$ and $^5D_0 \rightarrow {}^7F_2$ transitions of Eu^{3+}, respectively. For $LiBaB_9O_{15}$:0.02Tb^{3+} (b), the excitation spectrum of the samples consist of numbers of line excitation peaks (260 nm, 240 nm, 350 nm, 377 nm) among which 377 nm is the maximum, one assigned to the f-f transitions of Tb^{3+} $4f^8$ configuration. Under optimal excitation wavelength at 377 nm, the sample exhibits a green emission band with maximum emission at 551 nm, which originates from the 5d-4f transition of Tb^{3+} ions. The sharp lines at 491 nm, 551 nm, 590 nm and 623 nm are assigned to the $^5D_4 \rightarrow {}^7F_6$, $^5D_4 \rightarrow {}^7F_5$, $^5D_4 \rightarrow {}^7F_4$ and $^5D_3 \rightarrow {}^7F_3$ transitions of Tb^{3+} ions, respectively.

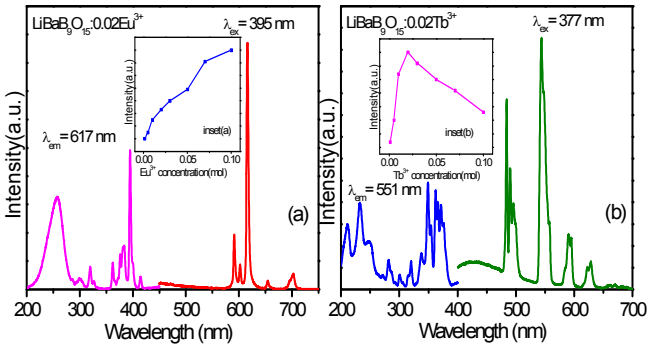

Figure 3 The PL and PLE spectra of $LiBaB_9O_{15}$:0.02Eu^{3+} (a) and $LiBaB_9O_{15}$:0.02Tb^{3+} (b); inset (a) shows the changes intensity with concentration in $LiBaB_9O_{15}$:yEu^{3+}, and inset (b) shows that in $LiBaB_9O_{15}$:xTb^{3+}

Figure 4(a) depicts the PLE spectrum of the Eu^{3+} ions singly doped phosphor, as well as the PL spectrum of the Tb^{3+} ions singly doped phosphor. To prove the probility of energy transfer from Tb^{3+} to Eu^{3+}, the rang of the PLE spectrum of the Eu^{3+} ions singly doped phosphor is strenched to 550 nm. While monitoring at 617 nm, a broad band ranging from 240 to 260 nm and some distinct peaks peaked at 377, 384, 395, and 460 nm exist in the excitation spectrum, which are attributed to Eu^{3+} absorption transitions. The PL spectrum of $LiBaB_9O_{15}$:0.02Tb^{3+} is also shown in Figure 4(a). The spectral overlap between the PL spectrum of $LiBaB_9O_{15}$:Tb^{3+} and the PLE spectrum of $LiBaB_9O_{15}$:Eu^{3+} is observed, which indicates that the energy transfer from the Tb^{3+} to Eu^{3+} ions may be expected in Tb^{3+} and Eu^{3+} codoped $LiBaB_9O_{15}$. According to Dexter's theory,[39] the effective resonance type energy transfer is expected to take place from Tb^{3+} to Eu^{3+} ions. This can be further confirmed by Figure 4 (b) (c) and (d), which shows the comparison of PLE spectra of $LiBaB_9O_{15}$:0.02Tb^{3+} monitored at 551 nm, $LiBaB_9O_{15}$:0.02Eu^{3+} monitored at 617 nm and $LiBaB_9O_{15}$:0.02Tb^{3+}, 0.02Eu^{3+} monitored at 617 nm, respectively. Compare Figure 4(c) with (d), the intensity ratio of 255 nm and 395 nm in $LiBaB_9O_{15}$:0.02Tb^{3+}, 0.02Eu^{3+} is larger that of in $LiBaB_9O_{15}$:0.02Eu^{3+}, which is the influence of Tb^{3+}. Also, the intensity ratio of 377 nm and 384 nm in $LiBaB_9O_{15}$:0.02Tb^{3+}, 0.02Eu^{3+} is larger that of in $LiBaB_9O_{15}$:0.02Eu^{3+}, which is the influence of Tb^{3+}. In addition, we can easily see that there is a peak at 350 nm in $LiBaB_9O_{15}$:0.02Tb^{3+}, 0.02Eu^{3+} and $LiBaB_9O_{15}$:0.02Tb^{3+}, which can not be seen from $LiBaB_9O_{15}$:0.02Eu^{3+}. In conclusion, compare Figure 4 (b), (c) and (d), the excitation spectrum (detected by the Eu^{3+} emission) has Tb^{3+} peaks, which demonstrating the occurrence of energy transfer from Tb^{3+} to Eu^{3+}. However, the energy transfer efficient is not so high that the influence of Tb^{3+} excitation is not obvious.

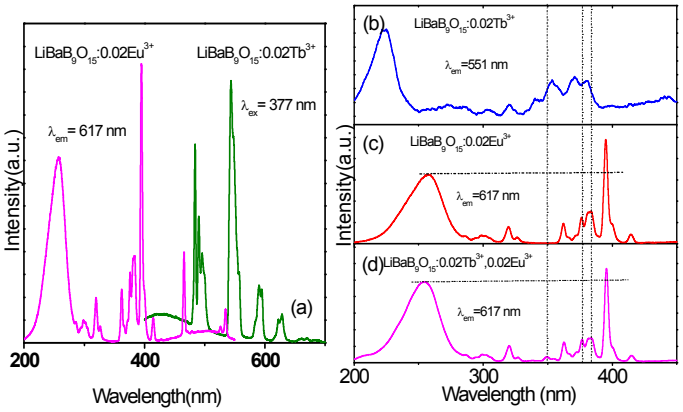

Figure 4 (a) The PL spectra of $LiBaB_9O_{15}$:0.02Tb^{3+} and the PLE spectra of $LiBaB_9O_{15}$:0.02Eu^{3+}; the comparison of PLE spectra of $LiBaB_9O_{15}$:0.02Tb^{3+} monitored at 551 nm (b), $LiBaB_9O_{15}$:0.02Eu^{3+} monitored at 617 nm (c) and $LiBaB_9O_{15}$:0.02Tb^{3+}, 0.02Eu^{3+} monitored at 617nm (d).

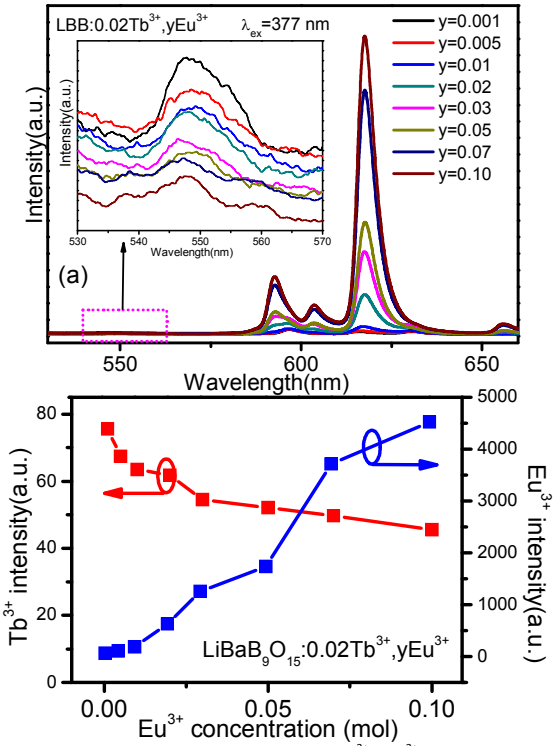

Figure 5 (a) The PL spectra of $LiBaB_9O_{15}$:0.02 Tb^{3+}, yEu^{3+}; inset is the enlarged figure from 530 nm to 570 nm; (b) the intensity of Tb^{3+} and Eu^{3+} in $LiBaB_9O_{15}$:0.02 Tb^{3+}, yEu^{3+} depending on Eu^{3+} concentration.

To deeply investigate the tunable PL properties of the $LiBaB_9O_{15}$ phosphor, we have codoped Eu^{3+} and Tb^{3+} ions with different relative concentrations into the $LiBaB_9O_{15}$ host lattice. The emission spectra of the Eu^{3+} and Tb^{3+} codoped $LiBaB_9O_{15}$ samples under the excitation at 377 nm are shown in Figure 5(a) and the inset, respectively. The codoped phosphor shows a green emission band of Tb^{3+} ions and a red emission band of Eu^{3+} ions at the irradiation of 377 nm. In principle, the color of the codoped phosphor should change from green to red with increase the concentration of Eu^{3+}, however, the fact is that it changes from pink to red. Also, compared with the emission of Eu^{3+}, the intrinsic emission from Tb^{3+} groups is very weak, suggesting that an efficient energy transfer from Tb^{3+} to Eu^{3+} occurred in the $LiBaB_9O_{15}$:0.02Tb^{3+}, *y*Eu^{3+} phosphors. Figure 5(b) show the intensity of Tb^{3+} and Eu^{3+} in $LiBaB_9O_{15}$:0.02 Tb^{3+}, *y*Eu^{3+} depending on Eu^{3+} concentration. The intensity of Tb^{3+} reduced with the increasing Eu^{3+} concentration. In contrast, the intensity of Eu^{3+} increased with the increasing Eu^{3+} concentration. The reason that the intensity of Tb^{3+} is reduced when the concentration of Tb^{3+} is a fixed value should be the energy transfer from Tb^{3+} to Eu^{3+}. The intensity of Eu^{3+} increased quickly with the increasing Eu^{3+} concentration proved the energy transfer from Tb^{3+} to Eu^{3+} laterally. Moreover, the energy transfer process is shown in Figure 6.

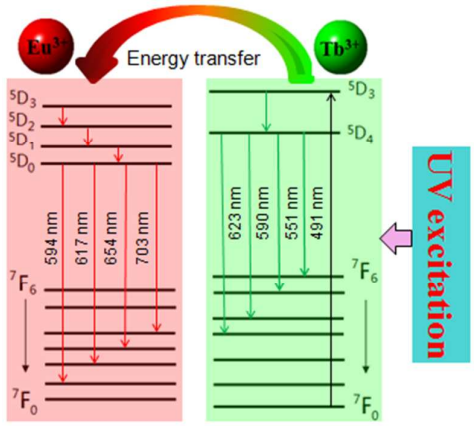

Figure 6 Energy transfer process

3.3. Energy transfer mechanism of $LiBaB_9O_{15}$:Tb^{3+}, Eu^{3+}

To support the spectrum analysis above, Figure 7 gives the fluorescence decay curves of Tb^{3+} and Eu^{3+} emissions by monitoring different emissions corresponding to the wavelengths at 551 nm and 617 nm in the $LiBaB_9O_{15}$:xTb^{3+}, 0.02Eu^{3+} and $LiBaB_9O_{15}$: 0.02 Tb^{3+}, yEu^{3+} phosphors. It is found that all of the decay curves show a second-order exponential decay, which can be fitted by the equation [41-43]

$$\mathbf{I(t) = I_0 + A_1 e^{-t/\tau 1} + A_2 e^{-t/\tau 2}} \quad (1)$$

The decay process of these samples is characterized by an average lifetime τ, which can be calculated using equation 2 as follows

$$\boldsymbol{\tau = (A_1 * \tau_1^{\,2} + A_2 * \tau_2^{\,2})/(A_1 * \tau_1 + A_2 * \tau_2)} \quad (2)$$

where I(t) is the luminous intensity at time t. On the basis of equation 2, the luminescence lifetimes of Tb^{3+} in $LiBaB_9O_{15}$:xTb^{3+}, 0.02 Eu^{3+} for different Eu^{3+} concentrations is shown in Figure 8(a). However, the luminescence lifetimes of Eu^{3+} in $LiBaB_9O_{15}$:0.02Tb^{3+}, yEu^{3+} for different Tb^{3+} concentrations is shown in Figure 8(b). The decrease in the lifetimes of Tb^{3+} with increasing Eu^{3+} concentration strongly demonstrates an energy transfer from Tb^{3+} to Eu^{3+}. In addition, the energy transfer efficiency (η_T) from Tb^{3+} to Eu^{3+} is calculated by the following equation[44]

$$\eta_T = 1 - \tau_s/\tau_{s0} \quad (3)$$

where τ_{s0} and τ_s represent the lifetime of Tb^{3+} in the absence and presence of Eu^{3+}, respectively. As shown in Figure 8(c), the energy transfer efficiencies increase gradually with increasing Eu^{3+} concentration and the energy transfer from Tb^{3+} to Eu^{3+} is efficient in the $LiBaB_9O_{15}$ host.

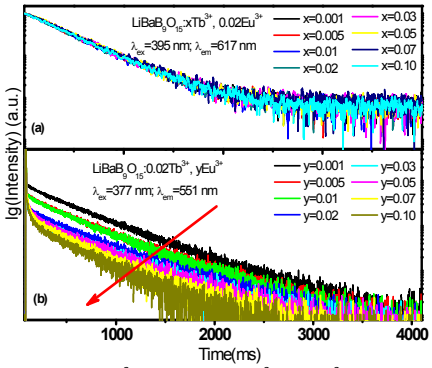

Figure 7 Decay curves of Eu^{3+} in $LiBaB_9O_{15}$:xTb^{3+},0.02Eu^{3+} (a) and decay curves of Tb^{3+} in $LiBaB_9O_{15}$:0.02Tb^{3+},yEu^{3+}.

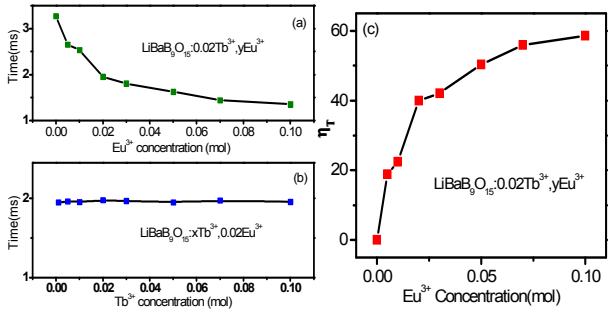

Figure 8 (a)The average decay time of Tb^{3+} in $LiBaB_9O_{15}$:0.02Tb^{3+}, yEu^{3+}; (b)the average decay time of Eu^{3+} in $LiBaB_9O_{15}$:xTb^{3+}, 0.02Eu^{3+} ; (c) the energy transfer efficiencies of $LiBaB_9O_{15}$:0.02Tb^{3+}, yEu^{3+}.

In general, energy transfer from the sensitizer to activator in a phosphor may take place via a multipolar interaction or an exchange interaction at higher concentrations. In order to determine the energy transfer mechanism in $LiBaB_9O_{15}$ samples, it is necessary to know the critical distance (R_c) between activator and sensitizer such as Eu^{3+} and Tb^{3+} here. With the increase of Tb^{3+} content, the distance between Eu^{3+} and Tb^{3+} ions becomes shorter,

thus the probability of energy migration increases constantly. When the distance is small enough, the concentration quenching occurs and the energy migration is hindered. Therefore, the calculation of R_C has been pointed out by Blasse[45-47]

$$R_c = 2[\frac{3V}{4\pi X_c N}]^{1/3} \quad (4)$$

where V corresponds to the volume of the unit cell, N is the number of host cations in the unit cell, and X_c is the total concentration of Tb^{3+} and Eu^{3+} ions when the emission intensity of Tb^{3+} ions is half of that in the same host in the absence of Eu^{3+} ions. For the $LiBaB_9O_{15}$ host, N=6, V=1782.59 Å^3, and X_c is 0.04 for Eu^{3+} and Tb^{3+}. Accordingly, the R_c was estimated to be about 24.2 Å. Moreover, when the value of Eu^{3+} takes 0.10, that is to say, X_c is 0.12 for Eu^{3+} and Tb^{3+}, the R_c was estimated to be about 16.8 Å. The results obtained above indicate the little possibility of exchange interaction since the exchange interaction is predominant only for about 5 Å indicating that the exchange interaction is not dominant. Thus the energy transfer from Tb^{3+} to Eu^{3+} may take place via the multipolar interaction.

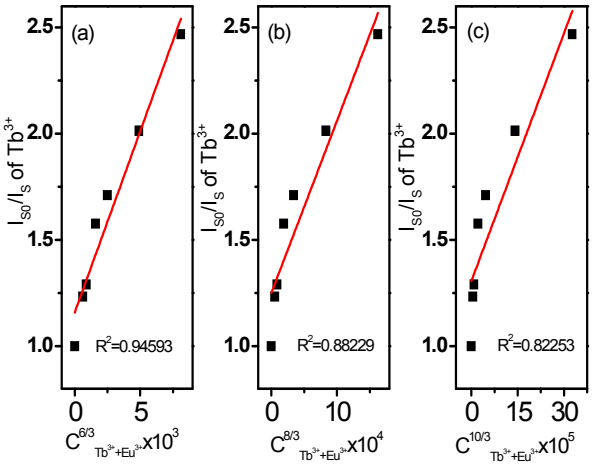

Figure 9 Dependence of (I_{S0}/I_S) of Tb^{3+} on (a) $C^{6/3}_{Tb^{3+}+Eu^{3+}}$, (b) $C^{8/3}_{Tb^{3+}+Eu^{3+}}$ and (c) $C^{10/3}_{Tb^{3+}+Eu^{3+}}$.

On the basis of Dexter's energy transfer formula of multipolar interactions and Reisfeld's approximation, the following relationship can be given[48]

$$\frac{\eta 0}{\eta s} \propto C^{n/3}_{Tb^{3+}+Eu^{3+}} \quad (5)$$

where η_0 and η_S are the luminescence quantum efficiencies of Tb^{3+} in the absence and presence of Eu^{3+}, respectively; the value of η_0/η_S can be approximately calculated by the ratio of related luminescence intensities as follows

$$\frac{I_0}{I_s} \propto C^{n/3}_{Tb^{3+}+Eu^{3+}} \quad (6)$$

where $C_{Tb^{3+}+Eu^{3+}}$ is the total doped concentration of Tb^{3+} and Eu^{3+} ions and n=6, 8, and 10, corresponding to dipole-dipole, dipole-quadrupole, and quadrupole-quadrupole interactions. The plots of (I_{S0}/I_S)-$C^{n/3}_{Tb^{3+}+Eu^{3+}}$ are further illustrated in Figure 9(a)-(c). The linear relationship is observed only as n=6, indicating that the dipole–dipole interaction is mainly responsible for the energy transfer from Tb^{3+} to Eu^{3+} in $LiBaB_9O_{15}$:0.02Tb^{3+}, yEu^{3+}.

3.4. Quantum efficiency and CIE chromaticity coordinates of $LiBaB_9O_{15}$:Tb^{3+}, Eu^{3+}

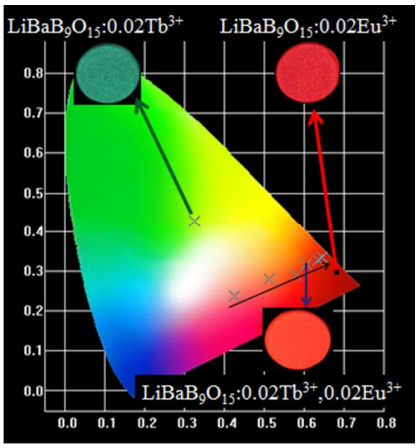

Figure 10 the CIE chromaticity coordinates (*x, y*) and photos for $LiBaB_9O_{15}$:0.02Tb^{3+}, yEu^{3+} phosphors.

Table 1 CIE (*x, y*) for $LiBaB_9O_{15}$:xTb^{3+}, 0.02Eu^{3+} phosphors

Samples	$LiBaB_9O_{15}$:xTb^{3+}, 0.02Eu^{3+}	CIE (*x, y*)
1	*x*=0.001	(0.6373, 0.3302)
2	*x*=0.005	(0.6416, 0.3336)
3	*x*=0.01	(0.6445, 0.3361)
4	*x*=0.02	(0.6379, 0.3342)
5	*x*=0.03	(0.6427, 0.3383)
6	*x*=0.05	(0.6408, 0.3405)
7	*x*=0.07	(0.6492, 0.3407)
8	*x*=0.10	(0.6432, 0.3412)

Figure 10 shows the CIE chromaticity coordinates (*x, y*) and photos for $LiBaB_9O_{15}$:0.02Tb^{3+}, yEu^{3+} phosphors. The CIE coordinates vary systematically from pink (*x*=0.4262, *y*=0.2370) to red (*x*=0.6478, *y*=0.3362) for $LiBaB_9O_{15}$:0.02Tb^{3+}, yEu^{3+} with the changes of Eu^{3+} ions concentration. Thus, the light color emission for $LiBaB_9O_{15}$:0.02Tb^{3+}, yEu^{3+} can be tuned from pink to red by adjusting the concentration of Tb^{3+} and Eu^{3+}. The CIE coordinates for $LiBaB_9O_{15}$:xTb^{3+}, 0.02Eu^{3+} phosphors is so close to the changes of Tb^{3+} ions concentration that we can't distinguish the points with each other in a chromaticity diagram, so we shows the CIE chromaticity coordinates (*x, y*) for $LiBaB_9O_{15}$:xTb^{3+}, 0.02Eu^{3+} phosphors in Table 1. When the value of *x* increases to 0.02 and *y* increases to 0.05, a red light can be obtained with good CIE coordinates of (0.6458, 0.3357). On the basis of the photoluminescence properties and energy transfer from Tb^{3+} to

Eu^{3+}, the $LiBaB_9O_{15}:Tb^{3+}$, Eu^{3+} phosphor might have potential applications as a red emitting phosphor for UV-excited white-LEDs.

Under 377 nm UV excitation, the quantum yields (QYs) of $LiBaB_9O_{15}:xTb^{3+}$, yEu^{3+} samples have been measured and listed in Table 2. The QE value can be calculated by the following equation:

$$\eta_{QE} = \frac{\int L_S}{\int E_R - \int E_S} \quad (7)$$

where L_S is the emission spectrum of the studied sample, E_S is the spectrum of the light used for exciting the sample, and E_R is the spectrum of the excitation light without the sample in the sphere. As we can see in Table 2, the maximum value can reach 45.0% for $LiBaB_9O_{15}:0.02Tb^{3+}$, $0.05Eu^{3+}$ and 51.5% for $LiBaB_9O_{15}:0.03Tb^{3+}$, $0.02Eu^{3+}$, respectively.

Table 2 The quantum efficiency (QE) of $LiBaB_9O_{15}$: xTb^{3+}, yEu^{3+} samples

$LiBaB_9O_{15}:0.02Tb^{3+}$, yEu^{3+}	QE (%)	$LiBaB_9O_{15}:xTb^{3+}$, $0.02Eu^{3+}$	QE (%)
y=0.02	29.3	x=0.02	44.2
y=0.03	39.0	x=0.03	51.5
y=0.05	45.0	x=0.05	39.4
y=0.10	36.2	x=0.10	15.9

4. Conclusions

In summary, a series of novel phosphor $LiBaB_9O_{15}:Tb^{3+}$, Eu^{3+} has been synthesized by a conventional high-temperature solid-state method at 850 °C for 2 h. Under 377 nm excitation, there is an efficient energy transfer from Tb^{3+} to Eu^{3+} via a dipole-dipole interaction mechanism. The critical distance of energy transfer from Tb^{3+} to Eu^{3+} is calculated to be 24.2 Å, and in this work the maximum efficiency of energy transfer in this concentration interval is about 58.60%. The emission color of phosphor $LiBaB_9O_{15}:Tb^{3+}$, Eu^{3+} can be tuned from pink to red by adjusting the concentration of Eu^{3+}. Moreover, the maximum value can reach 45.0% for $LiBaB_9O_{15}:0.02Tb^{3+}$, $0.05Eu^{3+}$ and 51.5% for $LiBaB_9O_{15}:0.03Tb^{3+}$, $0.02Eu^{3+}$, respectively. On the basis of luminescence properties and energy transfer from Tb^{3+} to Eu^{3+}, $LiBaB_9O_{15}:Tb^{3+}$, Eu^{3+} phosphor might have potential applications as a red emitting phosphor for UV-excited white-LEDs.

Acknowledgements

The work is supported by the National Natural Science Foundation of China (No.50902042), the Funds for Distinguished Young Scientists of Hebei Province, China (No.A2015201129), the Natural Science Foundation of Hebei Province, China (Nos.A2014201035, E2014201037), the Education Office Research Foundation of Hebei Province, China (Nos.ZD2014036, QN2014085), the Midwest Universities Comprehensive Strength Promotion Project.

Notes and references

1 C. H. Huang and T. M. Chen. J. Phys. Chem. C, 2011, 115, 2349-2355.
2 N. Guo, Y. J. Huang, H. P. You, M. Yang, Y. H. Song, K. Liu and Y. H. Zheng. Inorg. Chem., 2010, 49, 10907-10913.
3 Mengmeng Shang, Chunxia Li and Jun Lin. Chem. Soc. Rev., 2014, 43, 1372-1386.
4 Y. H. Won, H. S. Jang, W. B. Im, D. Y. Jeon and J. S. Lee. Appl. Phys. Lett., 2006, 89, 231909.
5 C. H. Huang, T. M. Chen, W. R. Liu, Y. C. Chiu, Y. T. Yeh and S. M. Jang. ACS Appl. Mater. Interfaces, 2010, 2, 259- 264.
6 S. Nakamura and G. Fasol. Springer: Berlin, Germany, 1996.
7 S. Nakamura. MRS Bull., 2009, 34, 101-107.
8 J. S. Kim, P. E. Jeon, Y. H. Park, J. C. Choi, H. L. Park, G. C. Kim and T. W. Kim. Appl. Phys. Lett., 2004, 85, 3696-3698.
9 Z. D. Hao, J. H. Zhang, X. Z hang, X. Y. Sun, Y. S. Luo, S. Z. Lu and X. J. Wang. Appl. Phys. Lett., 2007, 90, 261113.
10 R. J. Xie, N. Hirosaki and T. Takeda. Appl. Phys. Express., 2009, 2, 022401-022403.
11 C. F. Guo, J. Yu, X. Ding, M. Li, Z. Y. Ren and J. T. Bai. J. Electrochem. Soc., 2011, 158, J42-J46.
12 M. M. Shang, G. G. Li, X. J. Kang, D. M. Yang, D. L. Geng and J. Lin. ACS Appl. Mater. Interfaces, 2011, 3, 2738-2746.
13 G. G. Li, D. L. Geng, M. M. Shang, C. Peng, Z. Y. Cheng and J. Lin. J. Mater. Chem., 2011, 21, 13334-13344.
14 N. Guo, H. P. You, Y. H. Song, M. Yang, K. Liu, Y. H. Zheng, Y. J. Huang and H. J. Zhang. J. Mater. Chem., 2010, 20, 9061-9067.
15 H. S. Jang and D. Y. Jeon. Appl. Phys. Lett., 2007, 90, 41906.
16 Y. Q. Li, N. Hirosaki, R. J. Xie, T. Takeda and M. Mitomo. Chem. Mater., 2008, 20, 6704-6714.
17 Y. Q. Li, G. de With and H. T. Hintzen. J. Lumin., 2006, 116, 107-116.
18 M. Wierzbicka-Wieczorek, U. Kolitsch and E. Tillmanns. Eur. J. Mineral., 2010, 22, 245–258.
19 W. R. Liu, C. H. Huang, C. P. Wu, Y. C. Chiu, Y. T. Yeh and T. M. Chen. J. Mater. Chem., 2011, 21, 6869-6874.
20 H. Y. Jiao and Y. H. Wang. J. Electrochem. Soc., 2009, 156, J117-J120.
21 C. H. Huang, W. R. Liu and T. M. Chen. J. Phys. Chem. C, 2010, 114, 18698-18701.
22 G. Li, Y. Zhang, D. Geng, M. Shang, C. Peng, Z. Cheng and J. Lin. ACS Appl. Mater. Interfaces, 2012, 4, 296-305.
23 W. Lü, N. Guo, Y. Jia, Q. Zhao, W. Lv, M. Jiao, B. Shao and H. You. Inorg. Chem., 2013, 52, 3007-3012.
24 D. Geng, M. Shang, D. Yang, Y. Zhang, Z. Cheng and J. Lin. Dalton Trans., 2012, 41, 14042-14045.
25 D. Geng, G. Li, M. Shang, D. Yang, Y. Zhang, Z. Cheng and J. Lin. J. Mater. Chem., 2012, 22, 14262-14271.
26 D. Geng, M. Shang, Y. Zhang, H. Lian, Z. Cheng and J. Lin. J. Mater. Chem. C, 2013, 1, 2345-2353.
27 X. Zhang and M. Gong. Dalton Trans., 2014, 43, 2465-2472.
28 W.-R. Liu, C.-H. Huang, C.-W. Yeh, Y.-C. Chiu, Y.-T. Yeh and R.-S. Liu. RSC Adv., 2013, 3, 9023-9028.
29 G. Zhu, S. Xin, Y. Wen, Q. Wang, M. Que and Y. Wang. RSC Adv., 2013, 3, 9311-9318.
30 W. Lü, Z. Hao, X. Zhang, Y. Luo, X. Wang and J. Zhang. Inorg. Chem., 2011, 50, 7846-7851.

31 X. Chen, P. Dai, X. Zhang, C. Li, S. Lu, X. Wang, Y. Jia and Y. Liu. Inorg. Chem., 2014, 53, 3441-3448.
32 C. Guo, Z. Yang, J. Yu and J. H. Jeong. Appl. Phys. A, 2012, 108, 569-576.
33 H. Liu, Y. Luo, Z. Mao, L. Liao and Z. Xia. J. Mater. Chem. C, 2014, 2, 1619-1627.
34 M. Jiao, N. Gao, W. Lu, Y. Jia, W. Lv, Q. Zhao, B. shao and H. You. Dalton trans., 2013, 42, 12395-12402.
35 Z. Xu, C. Li, G. Li, R. Chai, C. Peng, D. Yang and J. Lin. J. Phys. Chem. C., 2010, 114, 2573-2582.
36 X. Liu, Y. Lü, C. Chen, S. Luo, Y. Zeng, X. Zhang, M. Shang, C. Li, and J. Lin. J. Phys. Chem. C. 2014, 118, 27516-27524.
37 H. Jiao, F. Liao, S. Tian, X. Jing. J. Electrochem. Soc., 2003, 150, H220-H224.
38 G. Blasse and A. Bril, J. Lumin., 1970, 3, 109-131.
39 G. Blasse. J. Lumin., 1976, 14, 231-233.
40 D. L. Dexter. J. Chem. Phys., 2004, 21, 836-850.
41 X. Liu, C. Li, Z. Quan, Z. Cheng and J. Lin. J. Phys. Chem. C, 2007, 111, 16601-16607.
42 X. Liu, L. Yan and J. Lin. J. Phys. Chem. C, 2009, 113, 8478-8483.
43 M. Yu, J. Lin and J. Fang. Chem. Mater., 2005, 17, 1783-1791.
44 M. Ilmer, B. Grabmaier and G. Blasse. Chem. Mater., 1994, 6, 204-206.
45 G. Blasse and B. Grabmaier. Luminescent materials, Springer, 1994.
46 G. Blasse. Phys. Lett. A, 1968, 28, 444-445.
47 Z. G. Xia, Y. J. Liang, D. Y. Yu, M. F. Zhang, W. Z. Huang, M. H. Tong, J. M. Wu and J. W. Zhao. Opt. Laser Technol., 2014, 56, 387-392.
48 R. Reisfeld and N. Lieblich-Soffer. J. Solid State Chem., 1979, 28, 391-395.